Bone Morphogenetic Protein 4 Induces Differentiation of Colorectal Cancer Stem Cells and Increases Their Response to Chemotherapy in Mice

YLENIA LOMBARDO,[*,‡] ALESSANDRO SCOPELLITI,[*,‡] PATRIZIA CAMMARERI,[‡] MATILDE TODARO,[*] FLORA IOVINO,[*] LUCIA RICCI–VITIANI,[§] GASPARE GULOTTA,[*] FRANCESCO DIELI,[‖] RUGGERO DE MARIA,[§,¶] and GIORGIO STASSI[*,‡]

[*]Department of Surgical and Oncological Sciences, [‖]Department of Biopathology and Biotechnology, University of Palermo, Palermo; [‡]Cellular and Molecular Oncology, Fondazione Salvatore Maugeri, Pavia; [§]Department of Hematology and Oncology, Istituto Superiore di Sanità, Rome; and [¶]Mediterranean Institute of Oncology, Catania, Italy

BACKGROUND & AIMS: The limited clinical response observed in many patients with colorectal cancer may be related to the presence of chemoresistant colorectal cancer stem cells (CRC-SCs). Bone morphogenetic protein 4 (BMP4) promotes the differentiation of normal colonic stem cells. We investigated whether BMP4 might be used to induce differentiation of CRC-SCs and for therapeutic purposes. **METHODS:** CRC-SCs were isolated from 25 tumor samples based on expression of CD133 or using a selection culture medium. BMP4 expression and activity on CRC-SCs were evaluated in vitro; progeny of the stem cells were evaluated by immunofluorescence, immunoblot, and flow cytometry analyses. The potential therapeutic effect of BMP4 was assessed in immunocompromised mice after injection of CRC-SCs that responded to chemotherapy (n = 4) or that did not (n = 2). **RESULTS:** CRC-SCs did not express BMP4 whereas differentiated cells did. Recombinant BMP4 promoted differentiation and apoptosis of CRC-SCs in 12 of 15 independent experiments; this effect did not depend on Small Mothers against decapentaplegic (Smad)4 expression level or microsatellite stability. BMP4 activated the canonical and noncanonical BMP signaling pathways, including phosphoInositide 3-kinase (PI3K) and PKB (protein kinase B)/AKT. Mutations in PI3K or loss of Phosphatase and Tensin homolog (PTEN) in Smad4-defective tumors made CRC-SCs unresponsive to BMP4. Administration of BMP4 to immunocompromised mice with tumors that arose from CRC-SCs increased the antitumor effects of 5-fluorouracil and oxaliplatin. **CONCLUSIONS: BMP4 promotes terminal differentiation, apoptosis, and chemosensitization of CRC-SCs in tumors that do not have simultaneous mutations in Smad4 and constitutive activation of PI3K. BMP4 might be developed as a therapeutic agent against cancer stem cells in advanced colorectal tumors.**

Keywords: Neoplasia; Colon Cancer; Drug Resistance; Tumor Resistance to Chemotherapy.

Cancer stem cells (CSCs), as a subpopulation of tumor cells, are able to reproduce the original human tumor in experimental animal models.[1–3] Colorectal (CR) CSCs initially were identified through the selection of $CD133^+$ cells.[1,4] Later, additional markers were proposed to enrich for CSCs in colorectal cancer, such as aldehyde dehydrogenase (ALDH), Leucine-rich repeat-containing G-protein coupled receptor 5, CD166, CD44, and nuclear β-catenin.[5–7] CRC-SCs can be expanded as tumor spheres in vitro using a serum-free medium containing epidermal growth factor and basic fibroblast growth factor. Such tumor spheres contain CSCs, cancer progenitors, and early precursors, representing the best characterized method to expand an enriched population of tumorigenic cells. In the presence of serum, these sphere cells display a gradual acquisition of colon epithelial markers, while losing the tumorigenic potential.[1,2] The relative insensitivity of CRC-SCs to chemotherapeutic drugs may explain the frequent failure of conventional treatments in advanced tumors.[2,8] Therefore, the availability of cell cultures enriched in CSCs appears to be a powerful tool for the development of more effective therapies.

Colonic epithelium undergoes continual regeneration sustained by colon stem cells located at the very base of the crypt.[9] Several signaling pathways regulate colon stem cell self-renewal and differentiation. Bone morphogenetic proteins (BMPs) are important players in the differentiation program of the normal gut. These cytokines act by defining a decreasing gradient from the intestine lumen toward the crypt, counteracting stem cell expansion outside the crypt, and promoting intestinal epithelial cell differentiation.[10–12] BMPs are a subgroup

Abbreviations used in this paper: AKT/PKB, AKT/protein kinase B; ALDH, aldehyde dehydrogenase; APC, adenomatous polyposis coli; BMP, bone morphogenetic protein; BMPR, bone morphogenetic protein receptor; CR, colorectal; CRC-SC, colorectal cancer stem cell; CSC, cancer stem cell; FBS, fetal bovine serum; 5-FU, 5-fluorouracil; GSK, glycogen synthase kinase; KREMEN1, kringle containing transmembrane protein 1; MSI, micro satellite instable; MSS, micro satellite stable; PI3K, phospholnositide 3-kinase; PTEN, Phosphatase and Tensin homolog; RT-PCR, reverse-transcription polymerase chain reaction; SDAC, sphere-derived adherent cells; SFRP4, secreted frizzled-related protein 4; Smad, Small Mothers against decapentaplegic; wt, wild type.

0016-5085/$36.00
doi:10.1053/j.gastro.2010.10.005

of the transforming growth factor-β superfamily members whose signaling modulates the transcription of target genes. Different combinations of type II receptors (BMPR2) with any one of the type I receptors (anaplastic lymphoma kinase [Alk]2, Alk3/BMPR1A, and Alk6/BMPR1B) determine the specificity for the ligands eliciting different biological processes.[13] The canonical BMP pathway occurs through type I receptor–mediated phosphorylation of Smad1, Smad5, and Smad8/R-Smad.[14] Two phosphorylated R-Smads form a heterotrimeric complex with a common Smad4 (co-Smad), which translocates to the nucleus and cooperates with other transcription factors to modulate target gene expression.[15]

The most convincing evidence for the involvement of BMPs in CRCs is the recent finding that up to 50% of individuals with juvenile polyposis carry germline mutations in either BMPR1A or Smad4 genes.[16,17] Moreover, recent data indicate that the BMP pathway is inactivated in the majority of sporadic CRCs.[18] This is supported further by a transgenic mouse model in which the inactivation of the BMP pathways leads to polyp formation and up-regulation of Wnt signaling.[19]

The BMP-BMPR signaling promotes the differentiation of normal and cancer stem cells in the neural system.[20,21] Thus, BMPs have been proposed for the therapy of glioblastoma.[20,21] Here, we show that BMP4 displays potent therapeutic activity against CRC-SCs, which can be targeted effectively with the combined use of chemotherapy.

Materials and Methods

Tissue Collection, Isolation, and Culture of Cancer Cells

Human CRC specimens were obtained from 25 patients (age range, 50–88 y) undergoing CR resection, in accordance with the ethical standards of the institutional committee. Histologic diagnosis was based on the morphologic microscopic features of tumor cells.

Tumor tissue was mechanically and enzymatically digested as previously described.[2,22] After magnetic $CD45^+$ cell depletion, the tumor digest was cultured in collagen-coated flasks in the presence of Dulbecco's modified Eagle medium supplemented with 10% fetal bovine serum (FBS) to obtain primary tumor cells, and in ultra-low adhesion flasks (Corning, Lowell, MA) in the presence of serum-free medium supplemented with epidermal growth factor (20 ng/mL) and basic fibroblast growth factor (10 ng/mL, both from Sigma-Aldrich, St. Louis, MO 63103, USA) to promote the growth of CSCs as spheres in 1–2 months.

To achieve the in vitro differentiation of CSCs, dissociated sphere cells were cultured in Dulbecco's modified Eagle medium supplemented with 10% FBS in adherent conditions. These cells were conventionally indicated as sphere-derived adherent cells (SDACs).

Magnetic Sorting and Flow Cytometry

See the Supplementary Materials and Methods section for more detail.

Immunohistochemistry

See the Supplementary Materials and Methods section for more detail.

Western Blotting

See the Supplementary Materials and Methods section for more detail.

Cell Viability

See the Supplementary Materials and Methods section for more detail.

Animals and Tumor Model

Five- to 6-week-old female ($nu+/nu^+$) mice were obtained from Charles River Laboratories (Milan, Italy) and maintained according to institutional guidelines of the University of Palermo Animal Care committee. Dissociated sphere cells (5×10^5) were injected subcutaneously with Matrigel GF reduced (BD Biosciences, Erembodegem, Belgium) at a 1:2 ratio in a total volume of 100 μL. Tumor size was calculated once a week up for to 18 weeks according to the following formula: $(\pi/6) \times$ larger diameter $\times$ (smaller diameter).[2]

For tumor xenografts treatments see the Supplementary Materials and Methods section.

Statistical Analysis

See the Supplementary Materials and Methods section for more detail.

Mutation Analysis and Quantitative Reverse-Transcription Polymerase Chain Reaction

See the Supplementary Materials and Methods section for more detail.

Results

BMP4 Is Widely Expressed in Colorectal Cancer Tissue but Not in CRC-SCs

We first phenotypically characterized CRC specimens by H&E, alcian blue staining, and by immunohistochemistry for the epithelial markers CK20 and CK7, the intestine-specific transcription factors CDX2 and β-catenin (Figure 1*A*). We also evaluated the microsatellite status and the presence of mutations in adenomatous polyposis coli (APC) and Smad4 genes (Supplementary Table 1). All CRC epithelial cells examined widely expressed BMP4, except for a few cells at the very base of the disrupted colon crypt (Figure 1*B*), where stem cells are known to be located.[9,23] Regardless of microsatellite status, BMP4 was undetectable in the $CD133^+$ cell population, whereas it was expressed clearly in the $CD133^-$

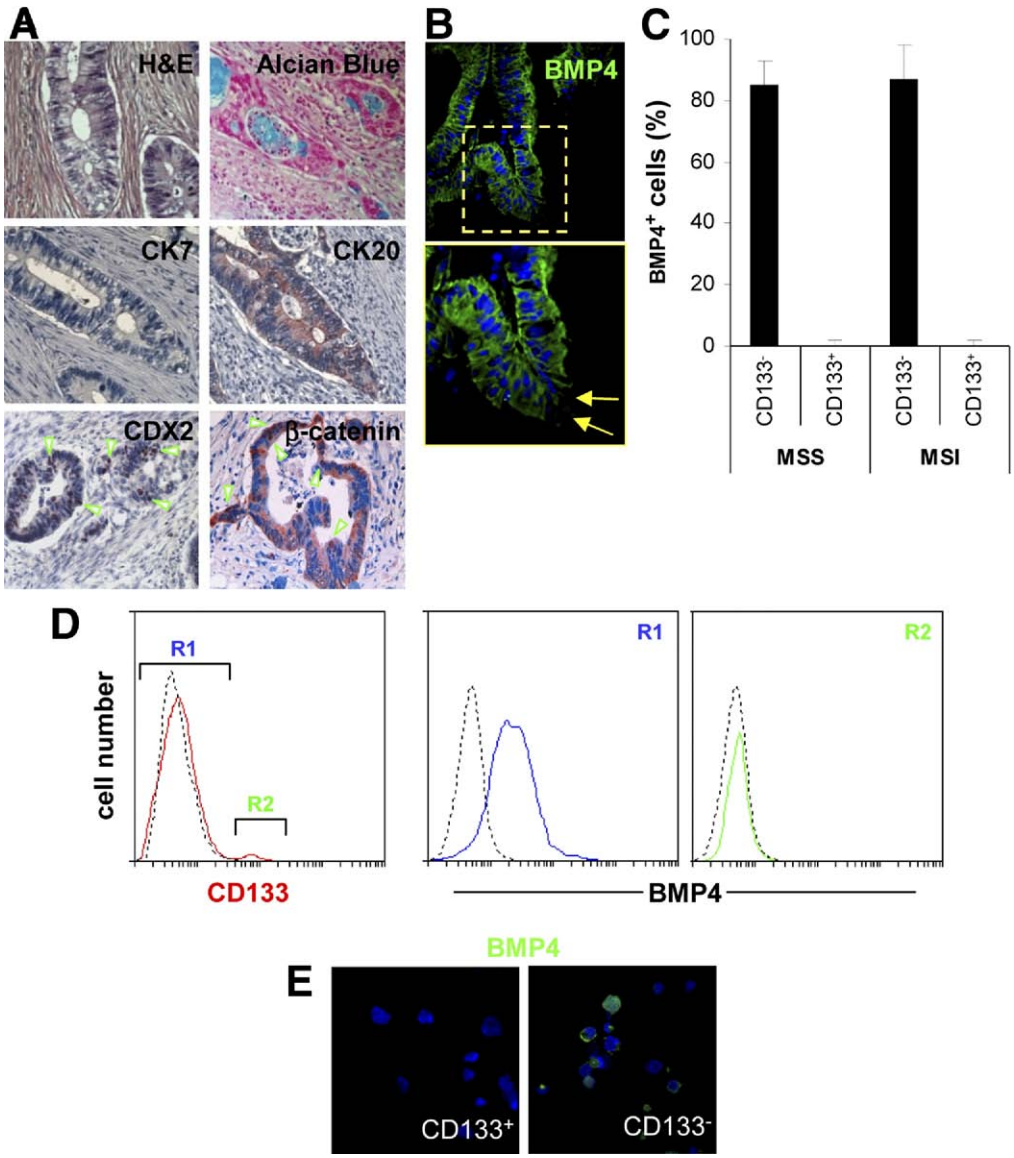

Figure 1. CD133$^+$ CRC-SCs do not express BMP4. (*A*) H&E and Alcian Blue staining (*upper panels*), immunohistochemical analysis for CK7 CK20 (*middle panels*), and CDX2 and β-catenin (*lower panels*) revealed by 3-amino-9-ethylcarbazol (*red color*) on paraffin-embedded sections. Nuclei are revealed by hematoxylin staining (*blue color*). One representative of 25 different tumors is shown. (*B*) Confocal microscopy analysis of BMP4 (*green color*) on optimal cutting temperature compound–embedded cryosections of CRC tissue. Nuclei were counterstained by Toto-3 (*blue color*). One representative of 25 different tumors is shown. (*C*) Percentage of BMP4$^+$cells evaluated by flow cytometry on CD133$^-$ and CD133$^+$ epithelial CRC cells. Data are expressed as mean ± SD of 11 MSS (patient numbers 10, 11, 13–15, 18, 19, and 22–25) and 5 MSI tumors (patient numbers 12, 16, 17, 20, and 21). (*D*) Representative flow cytometry profile of CD133 and BMP4 expression in CRC tumor cells as in *panel C*. (*E*) Representative immunofluorescence analysis of BMP4 (*green color*) on both CD133$^+$ and CD133$^-$ freshly purified cells from the sample as in *panel C*. Nuclei were counterstained by Toto-3 (*blue color*).

cell fraction (Figure 1*C–E*). These data show the absence of BMP4 expression in the CRC-SC fraction, suggesting a functional divergence with the differentiated cell compartment.

CRC-SCs can be isolated and successfully propagated in vitro as sphere cultures, allowing them to overcome the limit of the small amount of CD133$^+$cells in human tumor tissues.[2,7,22] We obtained sphere cultures from 25 CRC samples (Supplementary Table 1). Such CD133$^+$CRC spheres were analyzed for ALDH activity (Supplementary Figure 1*A*), which recently was shown to be a marker of tumorigenic CRC cells.[6,8] Irrespective of micro satellite instable (MSI) status, primary and SDACs displayed high levels of BMP4 expression, which conversely was undetectable in undifferentiated cells (Figure 2*A–D*). This confirmed that the expansion of CRC-SCs as spheres did not induce BMP4 expression, which instead was gradually gained during in vitro differentiation (Figure 2*E*). Comparable results were obtained inducing differentiation of CD133$^+$ freshly purified tumor cells (data not shown). Overall, these results suggest a potential role of this cytokine in the differentiation process.

BMP4 Signaling Pathway Can Be Switched On in CRC-SCs

All cancer specimens analyzed expressed of BMPR1A, BMPR1B, and BMPR2. A significant reduction of BMPR2 at both messenger RNA (mRNA) and protein levels was observed in spheres obtained from MSI samples (Figure 3*A* and *B*, and Supplementary Figure 1*B*). In line with BMP4 expression, differentiated CRC cells showed a constitutive active BMP canonical signaling, as revealed by the high levels of both p-Smad1-5-8 and Smad4 intermediate molecules in both micro satellite stable (MSS) and MSI tumors (Figure 3*C* and *D*). Exposure of sphere cells to BMP4 significantly increased the expression of Smad4, whereas

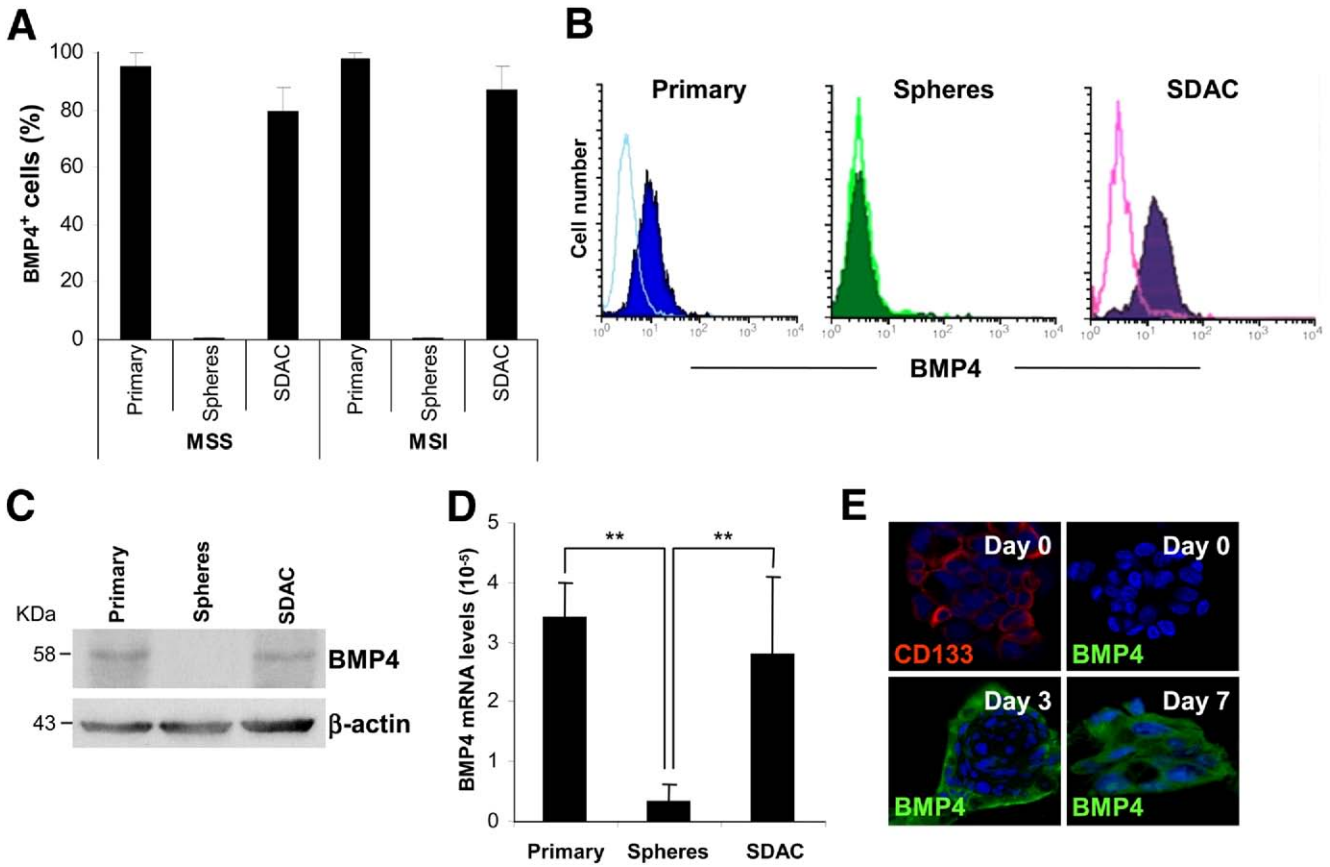

Figure 2. Expression of BMP4 in CRC primary cells, CSCs, and their differentiated progeny. (*A*) Percentage of BMP4$^+$ cells evaluated by flow cytometry in primary tumor cells (*Primary*), sphere cells (*Spheres*), and SDACs. Data are expressed as mean ± standard deviation of 10 MSS tumors (patient numbers 2–4, 10, 13–15, 11, 22, and 25) and 10 MSI tumors (patient numbers 3, 5–9, 12, 17, 20, and 21). (*B*) Representative flow cytometry analysis of BMP4 on samples as in *panel A*. (*C*) Representative immunoblot analysis of BMP4 on samples as in *panel A*. Loading control was assessed by β-actin. (*D*) BMP4 mRNA expression levels on primary tumor cells (*Primary*), sphere cells (*Spheres*), and SDACs. Columns represent the mean of 4 independent experiments ± standard deviation per group derived from 5 different patients. (*E*) Confocal microscopy analysis of CD133 (*red color*) or BMP4 (*green color*) on sphere cells exposed to 10% FBS for 0, 3, and 7 days. Nuclei were counterstained by Toto-3 (*blue color*). One representative of 20 experiments, each performed with spheres derived from a different patient, is shown. $^{**}P < .01$.

p-Smad1-5-8 was lower in MSI than in MSS CRC-SCs, as a possible consequence of the different levels of BMPR2 expression (Figure 3*C* and *D*). The activation of the BMP4 canonical pathway was confirmed by the prevalent p-Smad1,5,8 nuclear localization observed after BMP4 treatment in sphere cells from Smad4 wild-type tumors. This effect was not seen in Smad4 defective tumor samples (see Supplementary Table 1; indicated as Smad4-null) (Figure 3*E*).

BMP4 Induces Differentiation of CRC-SCs

Because BMP4 expression is restricted to differentiated cancer cells, we tested whether sphere cells can be

Figure 3. BMP4 administration activates the canonical signaling pathway in CRC-SCs. (*A*) mRNA expression of BMPR1A, BMPR1B, and BMPR2 on primary tumor cells (*Primary*), sphere cells (*Spheres*), and SDAC. (*B*) Relative quantification of BMPR1A, BMPR1B, and BMPR2 protein expression levels on samples as in *panel A*. Data in *panels A* and *B* are the mean ± standard deviation of 5 independent experiments, each performed with cells from 5 MSS (patient numbers 2, 4, 11, 13, and 22) and 5 MSI (patient numbers 3, 5, 8, 12, and 21) tumors. (*C*) Representative immunoblot analysis of pSmad1,5,8 and Smad4 on primary tumor cells (*Primary*), sphere cells (*Spheres*), SDACs, and spheres treated with BMP4 for 90 minutes. Samples shown are derived from 1 MSS (patient number 2) and 1 MSI (patient number 5) tumor. Loading control was assessed by β-actin. (*D*) Percentage of pSmad1,5,8$^+$ cells evaluated by flow cytometry in spheres untreated or treated with BMP4 for 90 minutes. Data are expressed as mean ± standard deviation of 5 MSS (patient numbers 2, 4, 11, 13, and 22) and 5 MSI (patient numbers 3, 5, 8, 12, and 21) tumor samples (*upper panel*). *Lower panel* shows a representative flow cytometry profile for pSmad1,5,8 of a MSS sample (patient number 4). (*E*) Representative confocal microscopy analyses for pSmad1,5,8 (*green color*) on sphere cells derived from 4 Smad4-wt MSS (patient numbers 2, 4, 11, and 13), 5 Smad4-wt MSI (patient numbers 3, 5, 8, 12, and 21), and 2 Smad4-null MSS tumors (patient numbers 14 and 22) treated as in *panel D*. Nuclei were stained with Toto-3 (*blue color*). $^{*}P < .05$; $^{**}P < .01$.

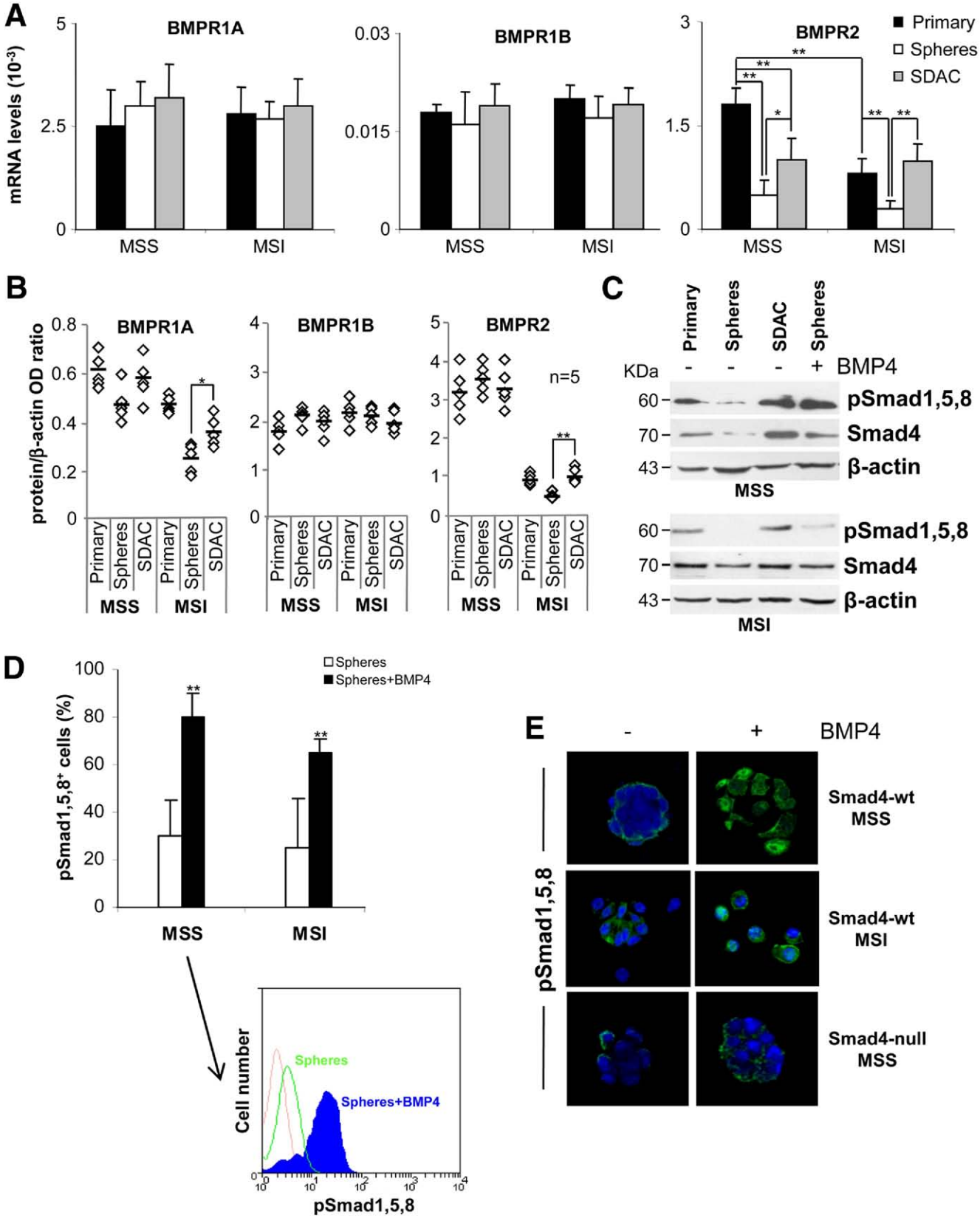
A
BMPR1A
BMPR1B
BMPR2
mRNA levels (10-3)
Primary
Spheres
SDAC
MSS
MSI
B
protein/β-actin OD ratio
n=5
C
KDa
+ BMP4
pSmad1,5,8
Smad4
β-actin
D
pSmad1,5,8+ cells (%)
Spheres+BMP4
Cell number
E
Smad4-wt MSS
Smad4-wt MSI
Smad4-null MSS

forced to differentiate upon exposure to the morphogenetic factor. CRC sphere cells were cultured in the presence of BMP4 or 10% FBS, which promotes the formation of differentiated cells expressing CK20 in about 2 weeks.[2] BMP4 administration induced a rapid differentiation of Smad4-wild type (wt) tumor CRC-SCs, as determined by plastic adherence and CK20 expression, which occurred considerably earlier than in FBS-treated cells. Phase-contrast microscopic analysis confirmed that BMP4 treatment was able to induce morphologic changes of CRC-SCs characterized by differentiation into large, polygonal colon cells, whereas noggin pretreatment abrogated BMP4 effects as revealed by the presence of floating $CK20^-$ sphere cells (Figure 4*A* and *B*). Although with slower kinetics, 4 of 7 Smad4-null tumor–derived CRC-SCs responded to the BMP4 pro-differentiation effect (Figure 4*A* and data not shown). The Smad4-null CRC-SCs (patient numbers 23–25) unresponsive to BMP4 maintained undifferentiated phenotype when treatment was protracted for 30 days (Figure 4*A* and *B*). In BMP4-responsive tumors, the presence of $CD133^+$, $ALDH^{high}$, and $ALDH1^+$ cells was reduced significantly after the treatment (Figure 4*C*, and Supplementary Figure 2*A*). Furthermore, BMP4 induced cell death in a significant portion of CRC-SCs (Figure 4*D*). Consistent with the concept that BMP4 induces differentiation, 48 hours exposure to BMP4 elicited a significant increase in the percentage of cells in the G0/G1 phase and a concomitant decrease in the percentage of cells in the G2/M phase as compared with untreated cells (Figure 4*E*, and Supplementary Figure 2*B*). The ability of BMP4 to differentiate CRC-SCs from 4 of 7 Smad4-defective tumors suggests the involvement of a noncanonical BMP pathway in the differentiation process.

BMP4 Inhibits the PI3K/AKT Signaling Pathway and Antagonizes Proliferative Effects of Wnt

BMP4 can trigger a noncanonical pathway that involves phosphoInositide 3-kinase (PI3K)/AKT activation and cross-talk between BMP4 and Wnt signaling.[11] We found that PTEN was scarcely expressed in CRC-SCs, but considerably increased during differentiation and after BMP4 treatment in all samples with a wild-type gene (Figure 5*A*–*C*, and Supplementary Figure 2*C*). By consequence, p-AKT and p-glycogen synthase kinase (GSK3)β levels were significantly higher in sphere cells as compared with primary tumor cells and SDAC. Activation of the PI3K/AKT signaling pathway was reduced significantly by BMP4 treatment in Smad4-wt and Smad4-null samples (patient numbers 14, 15, 19, and 22) (Figure 5*A* and *B*, and Supplementary Figure 2*C*). Intriguingly, BMP4 treatment did not affect the PI3K/AKT pathway of Smad4-null CRC-SCs unresponsive to BMP4-induced differentiation (patient numbers 23–25) (Figure 5*A*). The constitutive activation of this pathway was owing to an additional genetic alteration in PI3KCA (patient numbers 23 and 24) or the complete loss of PTEN (patient number 25) (Figure 5*C*). In BMP4-responsive samples including those harboring APC mutations (patient numbers 2, 4, 13, 15, and 17), BMP4 treatment reduced the expression levels of β-catenin and most importantly inhibited its nuclear translocation (Figure 5*D*). In accordance with previous data,[7] the PI3K inhibitor LY-294002 reduced the levels of nuclear β-catenin in sphere cells (Figure 5*D*). BMP4 induced an increased expression of E-cadherin, which binds to β-catenin and mediates epithelial cells adhesion and differentiation. Moreover, the treatment reduced cyclin D1 expression, which is required for cell-cycle G1/S transition (Figure 5*B*). Subsequently, we examined the levels of both canonical and stem cell Wnt targets by quantitative reverse-transcription polymerase chain reaction (RT-PCR). BMP4 treatment strongly reduced the expression levels of the direct Wnt targets axis inhibition protein 1, transcription factor Sp5, LGR5, and achaete-scute complex homolog 2, whereas the reduction of the robust marker for Lgr5-type stem cells olfactomedin 4[24] constituted additional evidence that BMP4 could target CSCs (Figure 5*E*).

A deeper analysis of the transcriptional profile of Wnt signaling in sphere cells after 48 hours of BMP4 treatment showed the down-regulation of 2 other Wnt targets, the transcription factor WNT1 inducible signaling pathway protein 1 and the regulator of growth Forkhead box N1, together with 13 Wnt-positive modulator ligands (Supplementary Figure 2*D*). In contrast, 2 negative regulators of Wnt-receptor signaling, kringle containing transmembrane protein 1 (KREMEN1) and secreted frizzled-related protein 4 (SFRP4), were clearly induced by BMP4 treatment (Figure 5*F*). Thus, our data suggest that different mechanisms converging in the shutdown of the Wnt pathway can be adopted by BMP4 to induce differentiation of CRC-SCs.

BMP4 Inhibits Tumorigenic Capacity of CRC-SCs

Sphere cells obtained from Smad4-wt (patient numbers 2 and 3), Smad4-null (patient numbers 14 and 15), and Smad4-null tumors with the PI3K/AKT pathway constitutively activated (patient numbers 24 and 25), were treated in vitro for 48 hours with BMP4 and then injected subcutaneously into immunocompromised mice. Injection of sphere cells gave rise to palpable tumors in about 3–4 weeks, which reproduced the same histopathology of the original human CRC. BMP4 pretreatment resulted in a considerable reduction in the capability of the majority of CRC-SC samples to grow in vivo, whereas this treatment was ineffective on Smad4-null CRC-SCs harboring PI3KCA mutation or loss of PTEN (Figure 6*A*). Consistent results were observed when 100 BMP4-saturated polyacrylic beads, at the site of engraftment, were injected weekly for 3 weeks after the injection of

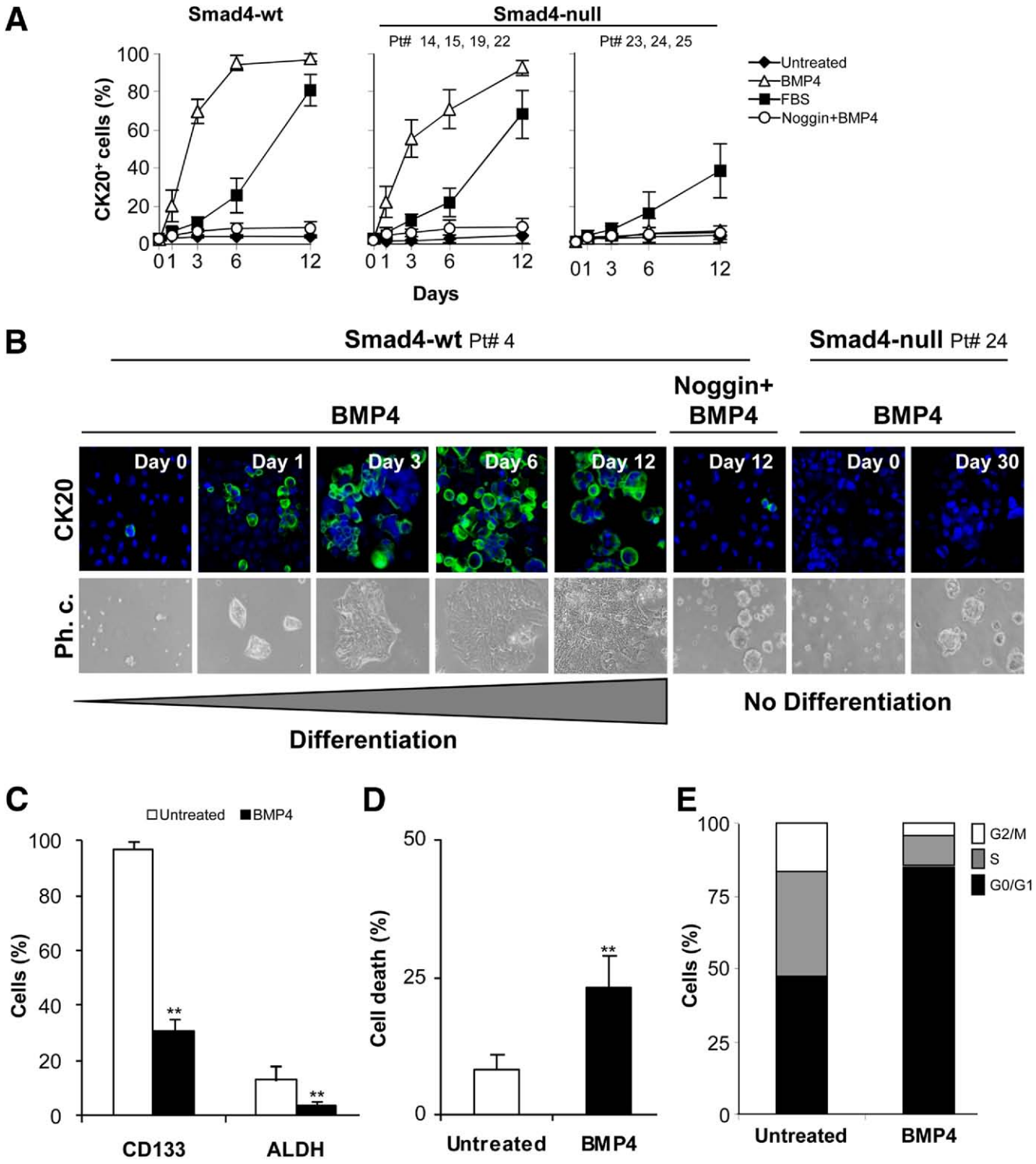

Figure 4. BMP4 promotes in vitro differentiation of CRC-SCs. (*A*) Percentage of CK20$^+$ dissociated sphere cells untreated or treated with BMP4, 10% FBS, or noggin plus BMP4. *Left panel* represents the mean ± standard deviation of 7 independent experiments performed on sphere cells from different Smad4-wt patients (patient numbers 2–4, 11–13, and 17). *Middle* and *right panels* show the mean ± standard deviation of 4 and 3 independent experiments, respectively, assessed on sphere cells derived from different Smad4-null patients (patient numbers 14, 15, 19, and 22–25). (*B*) Representative confocal microscopy analysis of CK20 (*green color*, *upper panels*) and phase-contrast microscopy (*lower panels*) of dissociated sphere cells derived from Smad4-wt tumors (patient number 4), treated with BMP4 alone or in combination with noggin for up to 12 days and from Smad4-null samples (patient number 24) treated with BMP4 for up to 30 days. Nuclei are stained in *blue*. (*C*) Percentage of CD133$^+$ and ALDH^{high} cells assessed by flow cytometry, on dissociated sphere cells untreated or treated with BMP4 for 6 days. (*D*) Cell death percentage of dissociated sphere cells untreated or treated with BMP4 for 48 hours. (*E*) Cell-cycle distribution of sphere cells treated as in *panel D*. (*C–E*) Data are mean ± SD of 10 independent experiments performed with cells from different samples (patient numbers 2–4, 11–15, 17, and 19). $^{**}P < .01$.

CRC-SCs harboring Smad4-wt and Smad4-null responsive to the BMP4 pretreatment. The therapeutic effect of BMP4 was abrogated by the concomitant administration of noggin. On the contrary, CRC-SCs treated with noggin alone generated tumors that grew even faster than tumors generated by control cells (Figure 6*B* and *C*).

We obtained similar results by injecting freshly sorted CD133$^+$ cells (patient numbers 13–16) pretreated in vitro

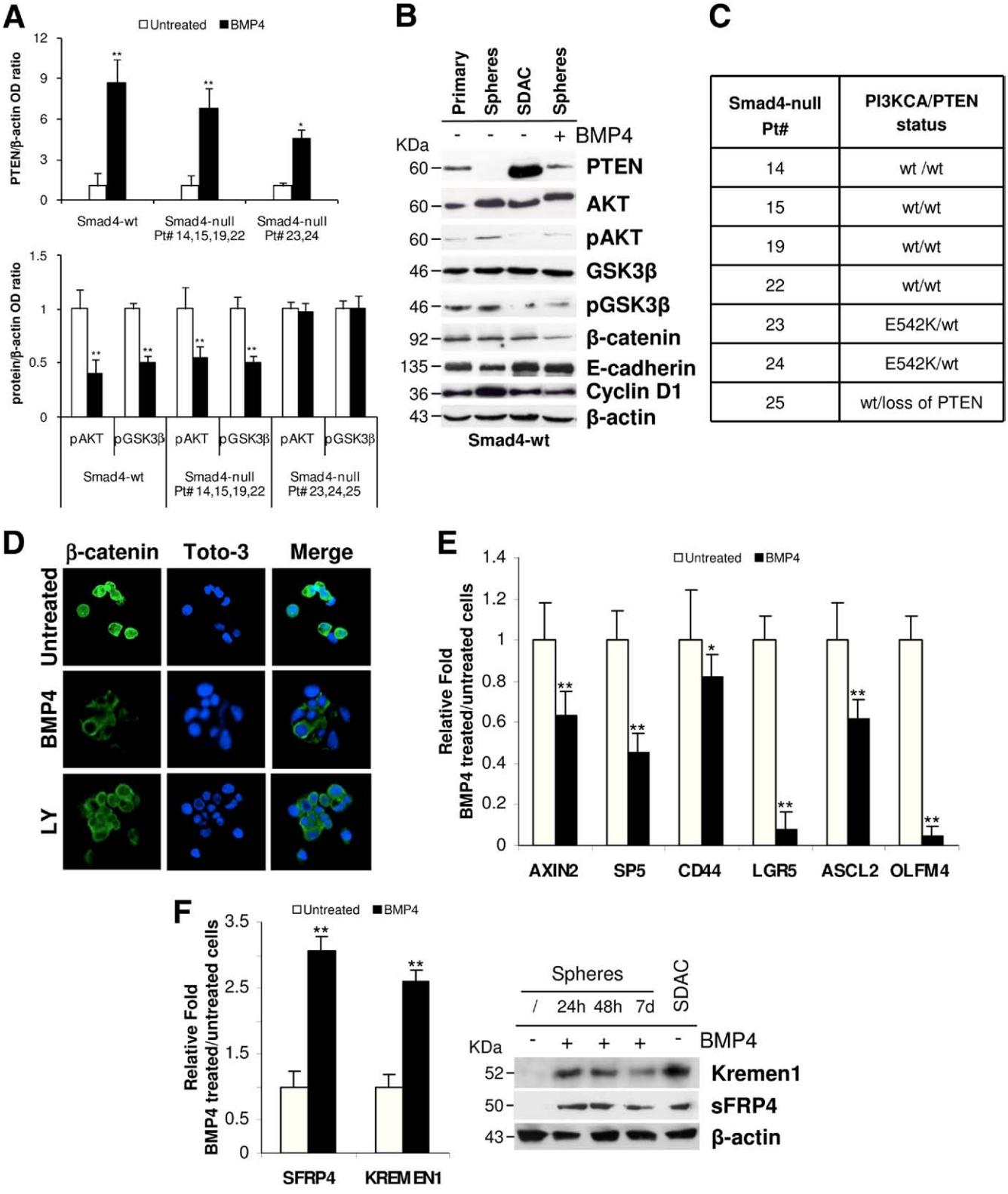

with BMP4 or post-treated in vivo using BMP4-saturated polyacrylic beads (data not shown).

Histologic examination showed that residual tumor xenografts generated by BMP4-treated CRC-SCs contained mainly dying cells and areas of fibrosis, highlighted by terminal deoxynucleotidyl transferase–mediated deoxyuridine triphosphate nick-end labeling and Azan Mallory staining, respectively (Figure 6*D*). The significant rate of cell death detected on BMP4-treated xenografts was consistent with the in vitro observations showing that BMP4-differentiated CSCs died because of their lifespan exhaustion. Moreover, BMP4-treated tumors contained a lower number of $CD133^+$ and $Ki67^+$ cells, confirming the in vivo prodifferentiation and antiproliferative effects of BMP4 (Figure 6*E* and *F*). Tumor xenografts obtained from the concomitant treatment of noggin and BMP4 showed histologic and antigenic profiles comparable with control tumors (Figure 6*D–F*). In contrast, a clear reduction of CK20 expression and significant increase of $CD133^+$ and $Ki67^+$ cells were observed in tumor xenografts generated by noggin-treated CRC-SCs (Figure 6*D–F*). Thus, BMP4 administration reduces growth and viability of colon cancer xenografts, suggesting that the strong inhibitory activity of BMP4 on CRC-SCs could be exploited for the therapy of CRC.

BMP4 Enhances the Cytotoxic Effects of Chemotherapy

Subcutaneously, tumors generated by sphere cell injection were exposed to oxaliplatin plus 5-fluorouracil (5-FU) alone or in combination with intratumoral injection of phosphate-buffered saline (PBS) or BMP4-loaded beads. Tumor response to chemotherapeutic drugs was enhanced by BMP4, whereas PBS or noggin pretreatment did not prevent tumor outgrowth. Specifically, the concomitant administration of BMP4 with oxaliplatin and 5-FU resulted in a marked antitumor effect, whereas oxaliplatin plus 5-FU alone only delayed tumor growth (Figure 7*A*). Furthermore, after the treatments were interrupted, tumor growth was abrogated only in the xenografts treated with BMP4 in combination with chemotherapy, resulting in a small fibrotic mass with a scarce cellularity, whereas a marked growth rate was observed in all the other tumors (Figure 7*B*). These data suggest that the combined treatment with chemotherapy and BMP4 results in a considerable therapeutic response that appears sustained after treatment interruption because CSCs are driven into differentiation and thereby eliminated.

Discussion

The failure to produce long-term clinical remission in CRC patients could reflect the inability to target CSCs efficiently, which are known to be resistant to conventional therapies.[2,8,25–27] Differentiation therapy, which results in a loss of self-renewal ability in CSCs and induction of terminal differentiation or apoptosis, may be a valid option for the treatment of CRC. Although this approach does not directly kill the cancer cells, it could make the conventional therapies more effective in the eradication of the tumor.

A well-established example of differentiation therapy is the use of all-trans retinoic acid in combination with chemotherapy in acute premyelocytic leukemia.[28] More recently, the prodifferentiation activity of BMPs has been proposed as a therapeutic option for human glioblastoma.[20,21]

In normal gut, BMP4 is not expressed at the base of the crypt owing to production of BMP antagonists by the myofibroblasts present in the stem cell niche, which allow the maintenance of Wnt activity and self-renewal of stem cells. Loss of these homeostatic mechanisms may contribute to tumor initiation.[12]

Our data show that BMP4 expression is limited to the differentiated progeny of CRC epithelial cells, which constitute the major population of the tumor mass. By contrast, BMP4 is undetectable in the CRC-SC fraction, which expresses the receptors BMPR1A, BMPR1B, and BMPR2. BMP canonical signaling can be activated by exogenous administration of BMP4 as revealed by the nuclear localization of pSmad1,5,8. This occurs even in MSI tumor-derived

Figure 5. BMP4 regulates the WNT pathway via PI3K/AKT signaling. (*A*) Densitometric analyses of the protein expression level of PTEN (*upper panel*), p-AKT, and p-GSK3β (*lower panel*) on sphere cells untreated or exposed to BMP4 for 48 hours. Data are mean ± standard deviation of independent experiments performed with cells derived from 7 Smad4-wt patients (patient numbers 2–4, 11, 13, 16, 17) and 7 Smad4-null patients (patient numbers 14, 15, 19, 22–25). (*B*) Western blot analysis of PTEN, AKT, p-AKT, GSK3β, p-GSK3β, β-catenin, E-cadherin, and cyclin D1 in primary tumor cells (*Primary*), sphere cells (Spheres), SDACs, and sphere cells treated as in *panel A*. Loading control was assessed by β-actin. One representative of 7 immunoblots for Smad4-wt tumors is shown. (*C*) PI3KCA and PTEN status in Smad4-null samples. Loss of PTEN expression was evaluated by Western blot and RT-PCR. (*D*) Confocal microscopy analysis of β-catenin (*green color*) on sphere cells treated with vehicle alone (*Untreated*), BMP4, or LY-294002 for 48 hours. Nuclei are stained by Toto-3 (*blue color*). One representative of 10 experiments performed using cells from different patients (patient numbers 2–4, 11, 13–17, and 19). (*E*) Relative fold of AXIN-2, SP5, CD44, LGR5, ASCL2, and OLFM4 gene expression levels in BMP4-treated vs untreated sphere cells. Data are expressed as mean ± standard deviation of 10 independent experiments, each performed with cells from samples as in *panel D*. (*F*) Relative fold of SFRP4 and KREMEN1 gene expression levels in BMP4-treated vs untreated sphere cells (*left panel*). Representative immunoblot analysis of SFRP4 and KREMEN1 on sphere cells untreated and treated with BMP4 up to 7 days and SDACs. Loading control was assessed by β-actin (*right panel*). Data are expressed as mean ± standard deviation of 10 independent experiments, each performed with cells from samples as in *panel D*. One representative of 5 immunoblots, each performed with cells from different patients (patient numbers 2, 3, 13, 14, and 15) is shown. $^*P < .05$; $^{**}P < .01$.

CSCs with reduced BMPR2 protein expression, suggesting that BMP4 may act through alternative type 2 receptors (ie, ACVR2 or transforming growth factor-βR2), and that the impaired function of a single receptor is not sufficient for complete pathway disruption.[29]

Substantiating the morphogenetic activity of this cytokine in intestinal cells, exposure to BMP4 leads to a rapid and massive CSC differentiation. Although previous reports showed that BMP administration induced apoptotic death in several systems,[10,30] we ob-

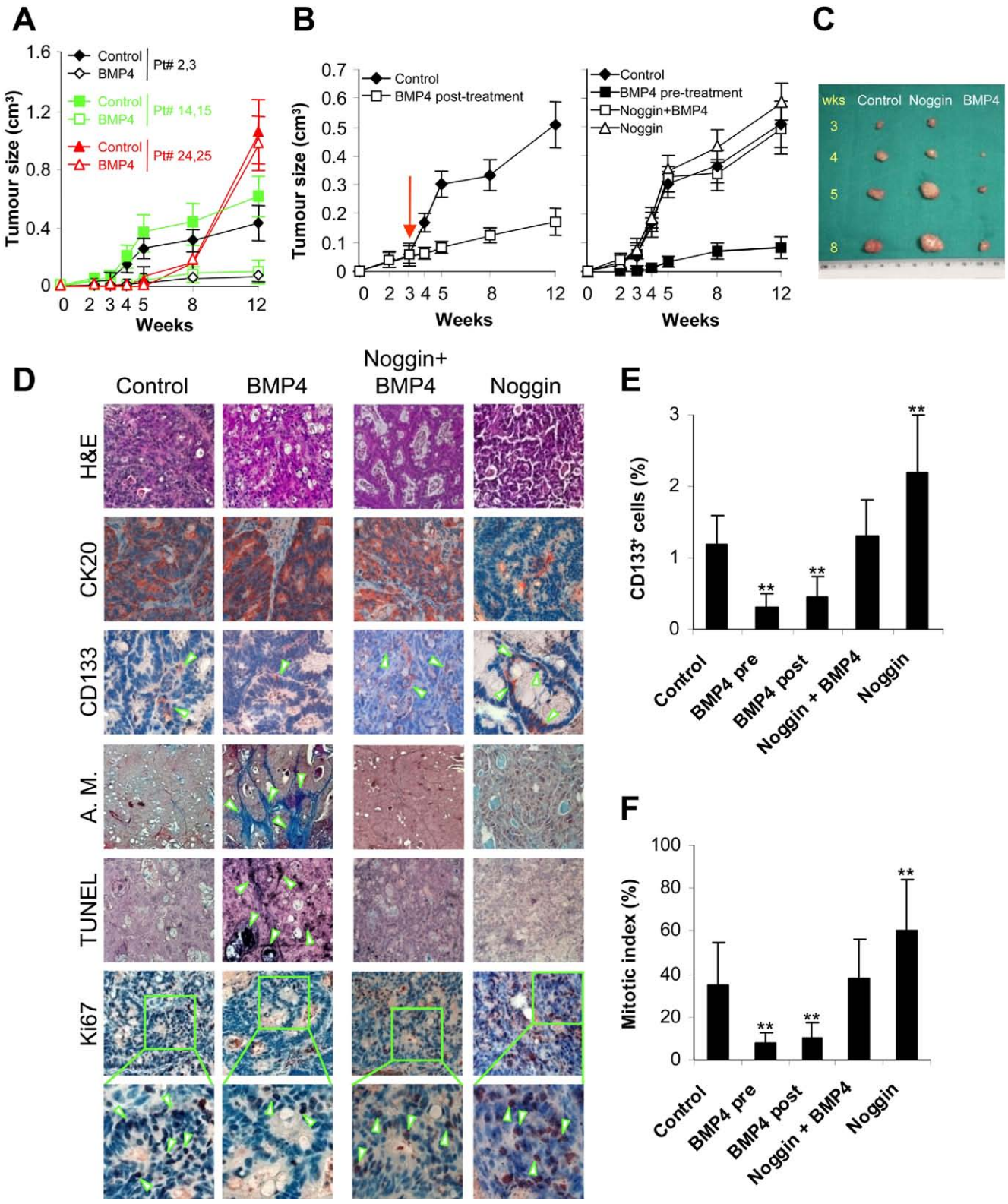

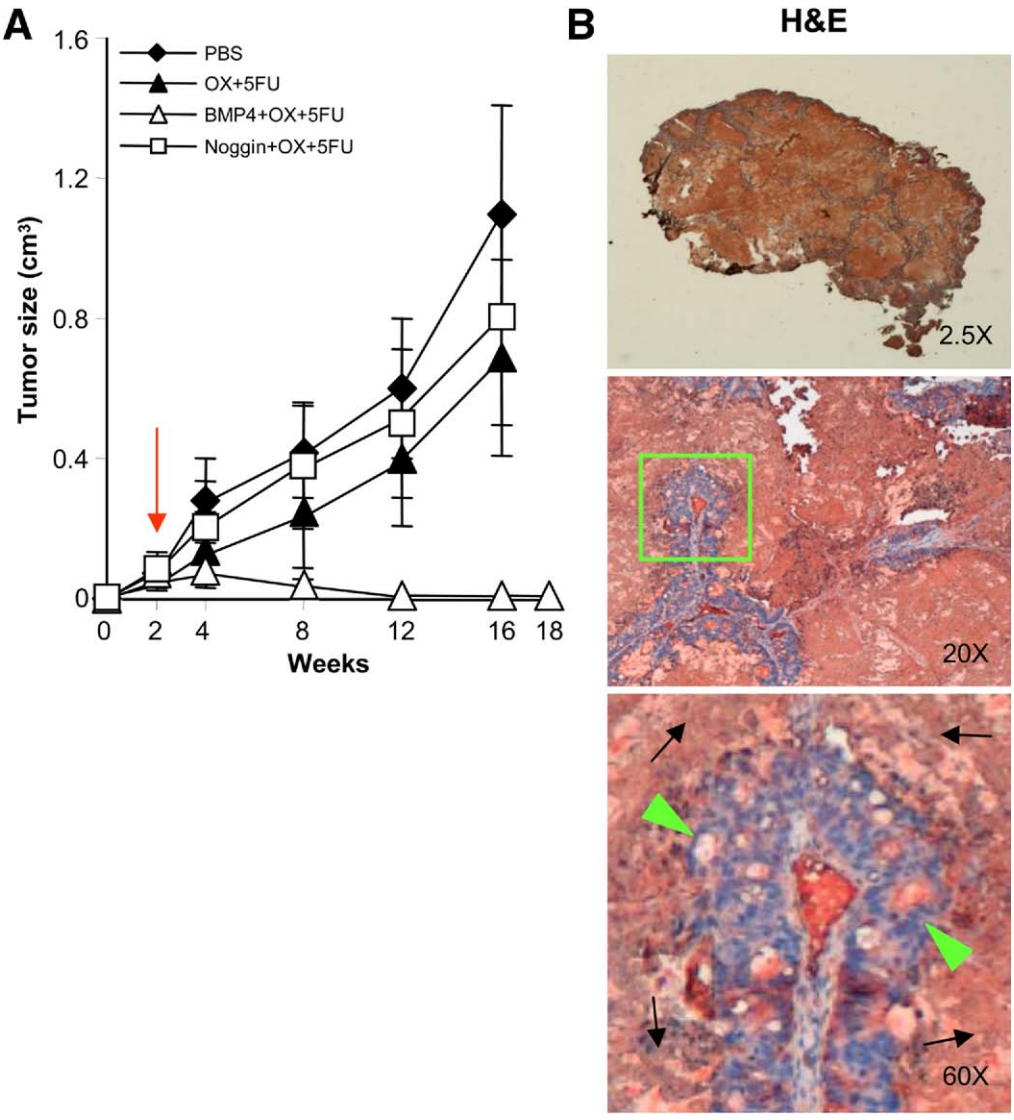

Figure 7. BMP4 enhances the cytotoxic effects of chemotherapy. (*A*) Size of subcutaneous xenografts derived from injection of untreated or noggin pretreated sphere cells, after intraperitoneal treatment with PBS or oxaliplatin plus 5-FU alone or combination with intratumoral injection of PBS- or BMP4-loaded beads. *Red arrow* indicates the starting point of treatment. Data are mean tumor size ± standard deviation of 4 independent sets of 5 tumors per group. Each set of tumors was obtained using cells from different donors (patient numbers 2, 3, 14, and 15). (*B*) Representative H&E staining of 20 xenografts after 6 weeks of treatment with oxaliplatin plus 5-FU in combination with BMP4-loaded beads. *Green* and *black arrowheads*, respectively, indicate the residual tumoral tissue and necrotic areas (magnification, 2.5×, 20×, 60×).

Figure 6. BMP4 reduces the tumorigenic potential of CRC-SCs. (*A*) Size of subcutaneous tumor growth after injection of dissociated sphere cells derived from 2 Smad4-wt (patient numbers 2 and 3), 2 Smad4-null (patient numbers 14 and 15), 1 Smad4-null/PI3KCA-mut (patient number 23), and 1 Smad4-null/PTEN-null (patient number 25) pretreated in vitro for 48 hours with vehicle (*Control*) or BMP4 (BMP4 *Pretreatment*). Data are mean tumor size ± standard deviation of 2 independent sets of 5 tumors per group. (*B*) Tumor size after intratumoral injection of polyacrylic beads, preadsorbed with vehicle alone (*Control*) or BMP4 (BMP4 *Post-treatment*). *Red arrow* indicates the starting point of treatments (*left panel*). Size of tumor growth after injection of dissociated sphere cells in vitro pretreated for 48 hours with vehicle (*Control*), BMP4 (BMP4 *Pretreatment*), noggin, or noggin + BMP4 (*right panel*). Data are mean tumor size ± standard deviation of 4 independent sets of 5 tumors per group. Each set of tumors was obtained using cells from different donors (Smad4-wt from patient numbers 2 and 3, and Smad4-null from patient numbers 14 and 15). (*C*) Representative set of xenografts derived from injection of dissociated sphere cells (Smad4-wt, patient number 3) pretreated in vitro with vehicle alone (*Control*), noggin, or BMP4 (BMP4 *Pretreatment*). (*D*) Representative H&E, Azan-Mallory, terminal deoxynucleotidyl transferase–mediated deoxyuridine triphosphate nick-end labeling (*Tunel*) (*dark blue color*) staining and immunohistochemical analyses for CK20, CD133, and Ki67 revealed by 3-amino-9-ethylcarbazol (*red color*) on paraffin-embedded section of xenografts, generated by sphere cells (Smad4-null, patient number 14), after treatment with vehicle alone, BMP4, noggin + BMP4, or BMP4 at 8 weeks (5 weeks of BMP4 post-treatment). Nuclei are revealed by hematoxylin staining (*blue color*). *Green arrowheads* indicate $CD133^+$ cells, fibrotic areas, dead cells, and $Ki67^+$ cells. (*E*) Percentage of $CD133^+$ cells evaluated on paraffin-embedded sections of tumors obtained after different treatments. (*F*) Mitotic index was calculated by nuclear expression of Ki67 reactivity as in *panel E*. (*E* and *F*) Mean ± SD of all 20 xenografts per group obtained at 8 weeks. Xenografts were generated by sphere cells derived from 2 Smad4-wt patients (patient numbers 2 and 3) and 2 Smad4-null patients (patient numbers 14 and 15). $^{**}P < .01$.

serve that the prevalent effect of BMP4 on CRC-SCs is G0/G1 accumulation followed by differentiation, with only a moderate induction of cell death. These results suggest that BMP4 exerts a prodifferentiative effect that prevents CSC expansion and triggers a differentiation program that may result in CSC depletion, thereby hampering tumor development.

We provide evidence that a non–Smad-dependent signaling pathway contributes to BMP4-mediated effects. In fact, BMP4 treatment increases PTEN levels and consequently inhibits the PI3K/AKT pathway in CRC-SCs. The simultaneous functional inactivation of Smad and the PI3K/AKT pathways makes CRC-SCs unresponsive to BMP4 treatment. Many studies have indicated that BMP stabilizes PTEN, thereby leading to reduced Akt activity.[31,32] These results are supported by the phenotype of PTEN mutant mice, which show similar tumors to those of noggin-transgenic mice, characterized by aberrant crypt fission and increased de novo crypt formation.[19,33] It has been reported that BMP signaling can inhibit Wnt activity, suppressing crypt formation in mouse models.[11,19] The connection between AKT and Wnt pathways is supported by the observed overactivation of β-catenin, which depends on the increased activity of AKT and 14-3-3ζ in the intestine stem cells of BMP-receptor type 1A knockout mice.[34] More recently, it was reported that BMP signaling can inhibit Wnt activity in mouse models resulting in suppressed crypt formation and reduced polyp growth,[11,19,35] and that high Wnt activity functionally designates the CRC-SCs.[36] We find that SFRP4 and KREMEN1, 2 negative regulators of Wnt signaling, are strongly up-regulated after BMP4 treatment. It has been shown that SFRPs, which we find to be regulated by BMP4, can potentially inhibit the entire canonical Wnt pathway even in colon cancers harboring mutations in CTNNB1 and APC.[37] Our results establish a roadmap of the signaling pathways (BMP4, PI3K/AKT, and Wnt) that control CSC tumorigenicity, whose investigation could allow the identification of specific molecular targets for future therapy.

The clinical benefit obtained by the combination of a prodifferentiation agent with chemotherapy in leukemia led us to propose the combination of BMP4 administration with current standard chemotherapy regimens for CRC. Our data show that the combined use of BMP4 with oxaliplatin and 5-FU is able to obtain complete long-term regression of CRC-SC tumor xenografts. Although the clinical use of such a combination would require the improvement of BMP4 delivery and optimization of the treatment schedule, the considerable enhancement of the therapeutic response obtained in mouse xenografts, even in long-term experiments, supports further investigations toward the use of differentiation therapy in CRC.

Supplementary Material

Note: To access the supplementary material accompanying this article, visit the online version of *Gastroenterology* at www.gastrojournal.org, and at doi: 10.1053/j.gastro.2010.10.005.

References

1. Ricci-Vitiani L, Lombardi DG, Pilozzi E, et al. Identification and expansion of human colon-cancer-initiating cells. Nature 2007; 445:111–115.
2. Todaro M, Alea MP, Di Stefano AB, et al. Colon cancer stem cells dictate tumor growth and resist cell death by production of interleukin-4. Cell Stem Cell 2007;1:389–402.
3. Hermann PC, Huber SL, Herrler T, et al. Distinct populations of cancer stem cells determine tumor growth and metastatic activity in human pancreatic cancer. Cell Stem Cell 2007;1:313–323.
4. O'Brien CA, Pollett A, Gallinger S, et al. A human colon cancer cell capable of initiating tumour growth in immunodeficient mice. Nature 2007;445:106–110.
5. Dalerba P, Dylla SJ, Park IK, et al. Phenotypic characterization of human colorectal cancer stem cells. Proc Natl Acad Sci U S A 2007;104:10158–10163.
6. Huang EH, Hynes MJ, Zhang T, et al. Aldehyde dehydrogenase 1 is a marker for normal and malignant human colonic stem cells (SC) and tracks SC overpopulation during colon tumorigenesis. Cancer Res 2009;69:3382–3389.
7. Vermeulen L, Todaro M, de Sousa Mello F, et al. Single-cell cloning of colon cancer stem cells reveals a multi-lineage differentiation capacity. Proc Natl Acad Sci U S A 2008;105:13427–13432.
8. Dylla SJ, Beviglia L, Park IK, et al. Colorectal cancer stem cells are enriched in xenogeneic tumors following chemotherapy. PLoS One 2008;3:e2428.
9. Barker N, van Es JH, Kuipers J, et al. Identification of stem cells in small intestine and colon by marker gene Lgr5. Nature 2007; 449:1003–1007.
10. Hardwick JC, Van Den Brink GR, Bleuming SA, et al. Bone morphogenetic protein 2 is expressed by, and acts upon, mature epithelial cells in the colon. Gastroenterology 2004;126:111–121.
11. He XC, Zhang J, Tong WG, et al. BMP signaling inhibits intestinal stem cell self-renewal through suppression of Wnt-beta-catenin signaling. Nat Genet 2004;36:1117–1121.
12. Kosinski C, Li VS, Chan AS, et al. Gene expression patterns of human colon tops and basal crypts and BMP antagonists as intestinal stem cell niche factors. Proc Natl Acad Sci U S A 2007;104:15418–15423.
13. Chen D, Ji X, Harris MA, et al. Differential roles for bone morphogenetic protein (BMP) receptor type IB and IA in differentiation and specification of mesenchymal precursor cells to osteoblast and adipocyte lineages. J Cell Biol 1998;142:295–305.
14. Miyazono K, ten Dijke P, Heldin CH. TGF-beta signaling by Smad proteins. Adv Immunol 2000;75:115–157.
15. Derynck R, Zhang YE. Smad-dependent and Smad-independent pathways in TGF-beta family signalling. Nature 2003;425:577–584.
16. Howe JR, Roth S, Ringold JC, et al. Mutations in the SMAD4/DPC4 gene in juvenile polyposis. Science 1998;280:1086–1088.
17. Howe JR, Bair JL, Sayed MG, et al. Germline mutations of the gene encoding bone morphogenetic protein receptor 1A in juvenile polyposis. Nat Genet 2001;28:184–187.
18. Kodach LL, Wiercinska E, de Miranda NF, et al. The bone morphogenetic protein pathway is inactivated in the majority of spo-

radic colorectal cancers. Gastroenterology 2008;134:1332–1341.
19. Haramis AP, Begthel H, van den Born M, et al. De novo crypt formation and juvenile polyposis on BMP inhibition in mouse intestine. Science 2004;303:1684–1686.
20. Piccirillo SG, Reynolds BA, Zanetti N, et al. Bone morphogenetic proteins inhibit the tumorigenic potential of human brain tumour-initiating cells. Nature 2006;444:761–765.
21. Chirasani SR, Sternjak A, Wend P, et al. Bone morphogenetic protein-7 release from endogenous neural precursor cells suppresses the tumourigenicity of stem-like glioblastoma cells. Brain 2010;133:1961–1972.
22. Cammareri P, Lombardo Y, Francipane MG, et al. Isolation and culture of colon cancer stem cells. Methods Cell Biol 2008;86:311–324.
23. Crosnier C, Stamataki D, Lewis J. Organizing cell renewal in the intestine: stem cells, signals and combinatorial control. Nat Rev Genet 2006;7:349–359.
24. van der Flier LG, Haegebarth A, Stange DE, et al. OLFM4 is a robust marker for stem cells in human intestine and marks a subset of colorectal cancer cells. Gastroenterology 2009;137:15–17.
25. Eramo A, Ricci-Vitiani L, Zeuner A, et al. Chemotherapy resistance of glioblastoma stem cells. Cell Death Differ 2006;13:1238–1241.
26. Cammareri P, Scopelliti A, Todaro M, et al. Aurora-a is essential for the tumorigenic capacity and chemoresistance of colorectal cancer stem cells. Cancer Res 2010;70:4655–4665.
27. Rich JN, Bao S. Chemotherapy and cancer stem cells. Cell Stem Cell 2007;1:353–355.
28. Nowak D, Stewart D, Koeffler HP. Differentiation therapy of leukemia: 3 decades of development. Blood 2009;113:3655–3665.
29. Kodach LL, Bleuming SA, Musler AR, et al. The bone morphogenetic protein pathway is active in human colon adenomas and inactivated in colorectal cancer. Cancer 2008;112:300–306.
30. Hallahan AR, Pritchard JI, Chandraratna RA, et al. BMP-2 mediates retinoid-induced apoptosis in medulloblastoma cells through a paracrine effect. Nat Med 2003;9:1033–1038.
31. Persad S, Troussard AA, McPhee TR, et al. Tumor suppressor PTEN inhibits nuclear accumulation of beta-catenin and T cell/lymphoid enhancer factor 1-mediated transcriptional activation. J Cell Biol 2001;153:1161–1174.
32. Waite KA, Eng C. From developmental disorder to heritable cancer: it's all in the BMP/TGF-beta family. Nat Rev Genet 2003;4:763–773.
33. He XC, Yin T, Grindley JC, et al. PTEN-deficient intestinal stem cells initiate intestinal polyposis. Nat Genet 2007;39:189–198.
34. Tian Q, He XC, Hood L, et al. Bridging the BMP and Wnt pathways by PI3 kinase/Akt and 14-3-3zeta. Cell Cycle 2005;4:215–216.
35. He XC, Zhang J, Li L. Cellular and molecular regulation of hematopoietic and intestinal stem cell behavior. Ann N Y Acad Sci 2005;1049:28–38.
36. Vermeulen L, De Sousa EMF, van der Heijden M, et al. Wnt activity defines colon cancer stem cells and is regulated by the microenvironment. Nat Cell Biol 2010;12:468–476.
37. Suzuki H, Watkins DN, Jair KW, et al. Epigenetic inactivation of SFRP genes allows constitutive WNT signaling in colorectal cancer. Nat Genet 2004;36:417–422.

Received January 22, 2010. Accepted October 4, 2010.

Reprint requests

Address requests for reprints to: Giorgio Stassi, MD, Department of Surgical and Oncological Sciences, Via Liborio Giuffrè 5, 90127 Palermo, Italy. e-mail: giorgio.stassi@unipa.it; fax: 0039 091 6553238.

Acknowledgments

Y.L. and A.S. contributed equally to this work.

Conflicts of interest

The authors disclose no conflicts.

Funding

This work was supported by grants from the Programmi di Ricerca Scientifica di Rilevante Interesse Nazionale (2007 project. 2007TE8NFY to G.S.), by grants from the Programma Straordinario di Ricerca Oncologica (Ministry of Health to G.S. and R.D.M. and Associazione Italiana per la Ricerca sul Cancro to M.T., G.S., and R.D.M.), and Y.L. was supported by an Investigator Fellowship from Collegio Ghislieri in Pavia, Italy.

Supplementary Materials and Methods

Magnetic Sorting and Flow Cytometry

Magnetic cell separation was performed on tumor digest using microbeads conjugated with CD45 or CD133/1 (AC133, mouse immunoglobulin [Ig]G1; Miltenyi, Bergisch Gladbach, Germany). Quality of sorting of both CD133+ and CD133- fractions was verified by flow cytometry with an antibody against CD133/2 (293C3-PE, mouse IgG1; Miltenyi).

Flow cytometry was performed using antibodies against CD133/2 (293C3-PE, mouse IgG2b; Miltenyi), CD133/1 (AC133, mouse IgG2b; Miltenyi), BMP4 (3H2, mouse IgG2b; Novocastra, Newcastle upon Tyne, UK), pSmad1,5,8 (rabbit polyclonal; CST, Pero-Milano, Italy), or isotype-matched controls. Sphere cells were treated with BMP4 (100 ng/mL; R&D Systems, Milano, Italy) for 90 minutes to evaluate pSmad1,5,8 expression. Reduction of CD133 expression was assessed after 6 days of BMP4 treatment.

ALDH enzymatic activity was evaluated on sphere cells untreated or treated with BMP4 for 6 days using the Aldefluor kit (Stem Cell Technologies) according to the manufacturer's instructions.

Cell-cycle analysis was performed on dissociated sphere cells untreated and treated with BMP4 for 48 hours, fixed in ice-cold 70% ethanol at 4°C overnight, and then incubated with PBS containing propidium iodide (50 μg/mL; Sigma), sodium citrate (3.8 M; Sigma), and RNase (10 μg/mL; Sigma) at 37°C for 30 minutes. Samples were analyzed using a flow cytometer (BD Biosciences).

Immunohistochemistry

Immunohistochemistry and/or immunofluorescence were performed on paraffin-embedded sections or cytospins as described.[1,2] The following antibodies were used: cytokeratin 7 (OVTL 12/30, mouse IgG1; DAKO Cytomation, Milano, Italy), cytokeratin 20 (Ks20.8, mouse IgG2a; DAKO Cytomation), CDX2 (CDX2-88 mouse IgG_1; Biocare, Concord, CA), β-catenin (H102, rabbit polyclonal; Santa Cruz Biotechnology, Santa Cruz, CA), BMP4 (3H2, mouse IgG1; Novocastra), CD133 (AC133, mouse IgG2b; Miltenyi), pSmad1,5,8 (rabbit polyclonal; CST), ALDH1 (44, mouse IgG1; BD Biosciences), Ki67 (MIB-1, mouse IgG1; Dako Cytomation), or isotype-matched controls. Immunofluorescence analysis of pSmad1,5,8 localization was performed on sphere cells untreated or treated with BMP4 for 48 hours.

To detect the proportion of differentiated and undifferentiated cells, dissociated spheres were cultured in stem cell medium in adherent conditions in the presence of BMP4 alone or in combination with noggin (300 ng/mL; R&D Systems) for up to 12 or 30 days. At different time points, the adherent cells were trypsinized and mixed with floating cells, cytospun, and stained for CK20. ALDH1 expression was evaluated after 6 days of BMP4 treatment.

Analysis of β-catenin localization was performed on sphere cells untreated or treated with BMP4 or LY-294002 (5 μmol/L, Calbiochem, Gibbstown, NJ) for 48 hours. A Nikon C1-Si confocal microscope (Nikon, Tokyo, Japan) was used to analyze fluorescence stainings.

For H&E, dewaxed sections were stained in hematoxylin (Sigma) for 5 minutes, washed in water, and then exposed for 1 minute to eosin (Sigma). For Azan Mallory, sections were stained with azocarmine G (Sigma) for 1 hour and with 5% of phosphovolframic acid for an additional hour. Then, sections were stained with aniline blue/orange G (Sigma) and mounted in synthetic resin. Alcian blue staining was performed with Alcian blue 8GX (Sigma) and counterstained with nuclear fast red (Lab Vision, Inc, Fremont, CA).

Apoptotic events were determined by terminal deoxynucleotidyl transferase–mediated deoxyuridine triphosphate nick-end labeling using the In Situ Cell Death Detection, AP Kit (Boehringer Mannheim, Ingelheim am Rhein, Germany). DNA strand breaks were detected by 5-bromo-4-chloro-3-indolyl-phosphate (BCIP, Dako Cytomation) substrate.

Western Blotting

Cell pellets were resuspended in ice-cold NP40 containing lysis buffer. Western blotting was performed as previously described.[2] Membranes were incubated with antibodies against BMP4 (3H2, mouse IgG2b; Novocastra), BMPR1A (87933, mouse IgG2b; R&D Systems), BMPR1B (88614, mouse IgG2a; R&D Systems), BMPR2 (73805, mouse IgG2b; R&D Systems), pSmad1,5,8 (rabbit polyclonal; CST), Smad4 (rabbit polyclonal; CST), PTEN (17A, mouse IgMk; Neomarkers, Fremont, CA), AKT (rabbit polyclonal; CST), pAKT (Ser 473, rabbit polyclonal; CST), GSK3β (rabbit polyclonal; CST), pGSK3β (Ser9, rabbit polyclonal; CST), cyclin D1 (DCS6, mouse IgG2a; CST), E-cadherin (rabbit polyclonal; CST), KREMEN1 (goat IgG; R&D Systems), SFRP4 (goat IgG; R&D Systems), β-catenin (H102, rabbit polyclonal; Santa Cruz Biotechnology), and β-actin (JLA20, mouse IgM; Calbiochem). Sphere cells were treated with BMP4 for 90 minutes to evaluate pSmad1,5,8 expression, for 48 hours to determine the effects on the PI3K/AKT pathway, or for up to 7 days for KREMEN1 and SFRP4 expression. Densitometry analyses were performed by Scion Image (Frederick, MD). Results were expressed as protein/β-actin optical density ratio.

Cell Viability

Cell viability was evaluated using the CellTiter Aqueous Assay Kit (Promega, Milano, Italy) on sphere cells untreated or treated with BMP4 for 48 hours, according to the manufacturer's instructions. Cell death

was evaluated by orange acridine (50 μg/mL)/ethidium bromide (1 μg/mL) staining.

Statistical Analysis

Statistical significance was determined by analysis of variance (1-way or 2-way) with a Bonferroni post-test. Results were considered significant when P values were less than .05. *Indicates $P < .05$ (Figure 3) whereas **indicates $P < .01$ (Figures 2–6).

Mutation Analysis

Genomic DNA was isolated from CRC tissue using the Wizard Genomic DNA Purification kit (Promega) according to the manufacturer's instructions. The DNA was used for PCR amplification of *APC* and *PI3KCA* genes. For the *APC* gene, the mutation cluster region was amplified as 5 overlapping fragments in a nested PCR strategy by using oligonucleotides and PCR condition previously published.[3] Amplification of the *PI3KCA* gene was performed using previously described primers.[4] For *SMAD4* mutation analysis, total RNA was subjected to reverse-transcription. The following overlapping *SMAD4* complementary DNA (cDNA) probes were used: *SMAD41F*-TTGATTTAAAAGGAAAAACTTGAACA, *SMAD41R*-TGCAGTCCTACTTCCAGTCCA, *SMAD42R*-GCAGAATGGATTTACTGGTCA, and *SMAD42F*-GGCCCGGTAAGTGAATTT.

PCR products were purified by the Microcon Montage PCR (Millipore, Billerica, MA) and then analyzed for sequence alterations with the Big Dye Terminator Cycle Sequencing kit (Applied Biosystems, Carlsbad, CA) using an ABI 3100 Genetic Analyzer (Applied Biosystems).

RNA Isolation and Real-Time PCR

Total RNA from the cell pellet was obtained using the RN easy Mini Kit (Qiagen GmbH; Valencia, CA), the residual amounts of DNA remaining were removed using RNase-Free DNase (Qiagen) according to the manufacturer's instructions. The yield of the extracted RNA was determined by measuring the optical density at 260 nm by Nanodrop ND-1000 (Nanodrop, Wilmington, DE). Total RNA (1 μg) was retrotranscribed using the High-Capacity cDNA Archive Kit (Applied Biosystems) according to the manufacturer's instructions. PCR amplification and detection of the PCR amplified gene products were performed with the SYBR Green PCR master mix (SuperArray Bioscience, Frederick, MD) or Taq Man master mix (Applied Biosystems). Levels of mRNA expression were quantified after normalization with endogenous control, glyceraldehyde-3-phosphate dehydrogenase, using the ΔCT (difference between Cycle threshold) method. Data processing and statistical analysis were performed using ABI PRISM SDS (software version 2.1; Applied Biosystems). For SYBR green chemistry, the following primers were purchased from MWG (Ebersberg, Germany): BMP4 forward primer 5′ CTG CCT GAT CTC AGC GGC ACC CAC ATC 3′, BMP4 reverse primer 5′ GCC GGA GGG CCA AGC GTA GCC CTA AG 3′, BMPR1A forward primer 5′ GTC ATA CGA AGA TAT GCG TGA GGT TGT 3′, BMPR1A reverse primer 5′ ATG CTG TGA GTC TGG AGG CTG GAT T 3, BMPR1B forward primer 5′ AAG GCT CAG ATT TTC AGT GTC GGG A 3′, BMPR1B reverse primer 5′ GGA GGC AGT GTA GGG TGT AGG TCT TTA TT 3′, BMPR2 forward primer 5′ GTG ACT GGG TAA GCT CTT GCC GTC T 3′, BMPR2 reverse primer 5′ GCA GGT TTA TAA TGA TCT CCT CGT GGT 3′, glyceraldehyde-3-phosphate dehydrogenase forward primer 5′ GCT TCG CTC TCT GCT CCT CCT GT 3′, and glyceraldehyde-3-phosphate dehydrogenase reverse primer 5′ TAC GAC CAA ATC CGT TGA CTC CG 3′. For Taq Man Probe detection, the following primers were purchased from Applied Biosystems: transcription factor Sp5 (Hs01370227_mH), axis inhibition protein 1 (Hs01063168_m1), CD44 (Hs00153304_m1), Lgr5 (Hs00969428_m1), and achaetescute complex homolog 2 (Hs00270888_s1).

PCR Array

The RT[2] Profiler PCR array was used to simultaneously examine the mRNA levels of 89 genes closely associated with Wnt pathway, including 5 housekeeping genes in 96-well plates, following the manufacturer's protocol (APHS-043C; SuperArray Bioscience). Briefly, cDNAs were synthesized from 1 μg of total RNA using the PCR Array First Strand cDNA Synthesis Kit (SuperArray Bioscience) according to the manufacturer's instructions.

Arrays were performed independently for each cell line and at least 3 technical replicates were run for each treated sample and controls.

Reverse transcriptase was inactivated by heating at 95°C for 5 minutes, and the cDNA was diluted to 100 μL by adding RNase-free water and stored at −20°C. cDNA was used as a template for PCR array using a SYBR Green PCR master mix (SuperArray Bioscience). For each 96-well plate of the PCR Array, a 2450-μL PCR master mix containing 1× PCR master mix and 98 μL of diluted cDNA was prepared, and an aliquot of 25 μL was added to each well. For quality control, no reverse-transcription control and no template control were performed. Amplification was performed using the following conditions: 10 minutes at 95°C, 15 seconds at 95°C, and 1 minute at 60°C for 40 cycles.

PCR was performed using an ABI 7900 HT FAST instrument (Applied Biosystems). Cycle threshold values were calculated for all the genes present on the array and normalized using the average of 5 housekeeping genes on the same array (B2M, HPRT1, RPL13A, glyceraldehyde-3-phosphate dehydrogenase, and actin B). The comparative cycle threshold method was used to calculate the relative quantification of

gene expression (sphere cells treated with BMP4 vs untreated sphere cells).

Tumor Xenograft Treatments

Pretreatment of sphere cells was performed by adding BMP4 (100 ng/mL), noggin (300 ng/mL), or noggin + BMP4 to growth medium for 48 hours before transplantation. Post-treatment of palpable tumors was performed by weekly intratumoral injection of 100 BMP4-coated beads for 9 weeks. Heparin acrylic beads (Sigma) were incubated with PBS or BMP4 (0.65 μg/μL) for 1 hour at 37°C.

Histologic examinations of xenografts were determined 8 weeks after cell injection on a minimum of 12 sections per tumor.

Chemotherapy sensitization was assessed on well-established tumors generated by subcutaneous injection of sphere cells treated with vehicle or noggin (300 ng/mL). Six mice per group were treated intraperitoneally with oxaliplatin (0.25 mg/kg once a week for 4 weeks) and 5-FU (15 mg/kg/day for 5 days a week for 2 weeks) alone or in combination with intratumoral injection of 100 BMP4-coated beads (once a week for 6 weeks). Controls were injected with beads loaded with PBS and intraperitoneal PBS.

References

1. Cammareri P, Lombardo Y, Francipane MG, et al. Isolation and culture of colon cancer stem cells. Methods Cell Biol 2008;86: 311–324.
2. Todaro M, Alea MP, Di Stefano AB, et al. Colon cancer stem cells dictate tumor growth and resist cell death by production of interleukin-4. Cell Stem Cell 2007;1:389–402.
3. Smith G, Carey FA, Beattie J, et al. Mutations in APC, Kirsten-ras, and p53–alternative genetic pathways to colorectal cancer. Proc Natl Acad Sci U S A 2002;99:9433–9438.
4. Samuels Y, Wang Z, Bardelli A, et al. High frequency of mutations of the PIK3CA gene in human cancers. Science 2004;304:554.

Supplementary Table 1. Case Description and Tumor Features

							CD133+		Spheres	
Case	Age/Sex	Site	Dukes	MSI	APC status	SMAD4 status	In vitro	In vivo	In vitro	In vivo
P1	65/M	Rectosigmoid	B	MSI	3927_{del}, STOP@1313	WT	—	—	Yes	—
P2	66/F	Rectosigmoid	C	MSS	4312_{del}, STOP@1453	WT	—	—	Yes	Yes
P3	65/F	Sigma	D	MSI	WT	WT	—	—	Yes	Yes
P4	57/F	Left	D	MSS	4132C>T, Gln1378STOP	WT	—	—	Yes	—
P5	63/M	Rectosigmoid	B	MSI	3955_{del}, STOP@1320	WT	—	—	Yes	—
P6	68/M	Rectosigmoid	D	MSI	4661ins, STOP@1558	WT	—	—	Yes	—
P7	57/M	Rectosigmoid	C	MSI	4261_{del}, STOP@1472	WT	—	—	Yes	—
P8	56/F	Sigma	D	MSI	4261del, STOP@1472	WT	—	—	Yes	—
P9	68/M	Rectosigmoid	D	MSI	3907C>T, Glu_{1303}STOP	WT	—	—	Yes	—
P10	56/F	Left	D	MSS	3925G>T, Glu_{1309}STOP	WT	Yes	—	Yes	—
P11	67/F	Rectosigmoid	A	MSS	WT	WT	Yes	—	Yes	—
P12	69/M	Sigma	C	MSI	3907C>T, Glu_{1303}STOP	WT	Yes		Yes	—
P13	57/M	Rectosigmoid	C	MSS	3905_{ins}, STOP@1304	WT	Yes	Yes	Yes	—
P14	67/M	Rectum	C	MSS	WT	R361C	Yes	Yes	Yes	Yes
P15	61/M	Sigma	C	MSS	4479_{del}, STOP@1506	Loss of Smad4[a]	Yes	Yes	Yes	Yes
P16	52/M	Rectum	B	MSI	WT	WT	Yes	Yes	Yes	—
P17	72/M	Sigma	C	MSI	4381G>T, Glu_{1461}STOP	WT	Yes	—	Yes	—
P18	55/F	Left	C	MSS	4185_{ins}, STOP@1397	WT	Yes	—	Yes	—
P19	68/M	Rectosigmoid	B	MSS	WT	Loss of Smad4[a]	Yes	—	Yes	—
P20	59/M	Rectum	C	MSI	WT	WT	Yes	—	Yes	—
P21	66/F	Right	B	MSI	WT	WT	Yes	—	Yes	Yes
P22	56/F	Left	D	MSS	3925G>T, Glu_{1309}STOP	Loss of Smad4[a]	Yes	—	Yes	Yes
P23	67/F	Sigma	C	MSS	WT	R361C	Yes	—	Yes	Yes
P24	68/M	Sigma	C	MSS	WT	R361C	Yes	—	Yes	Yes
P25	88/F	Rectum	B	MSS	WT	R361C	Yes	—	Yes	Yes

[a]Loss of Smad4 expression evaluated by Western blotting and RT-PCR.

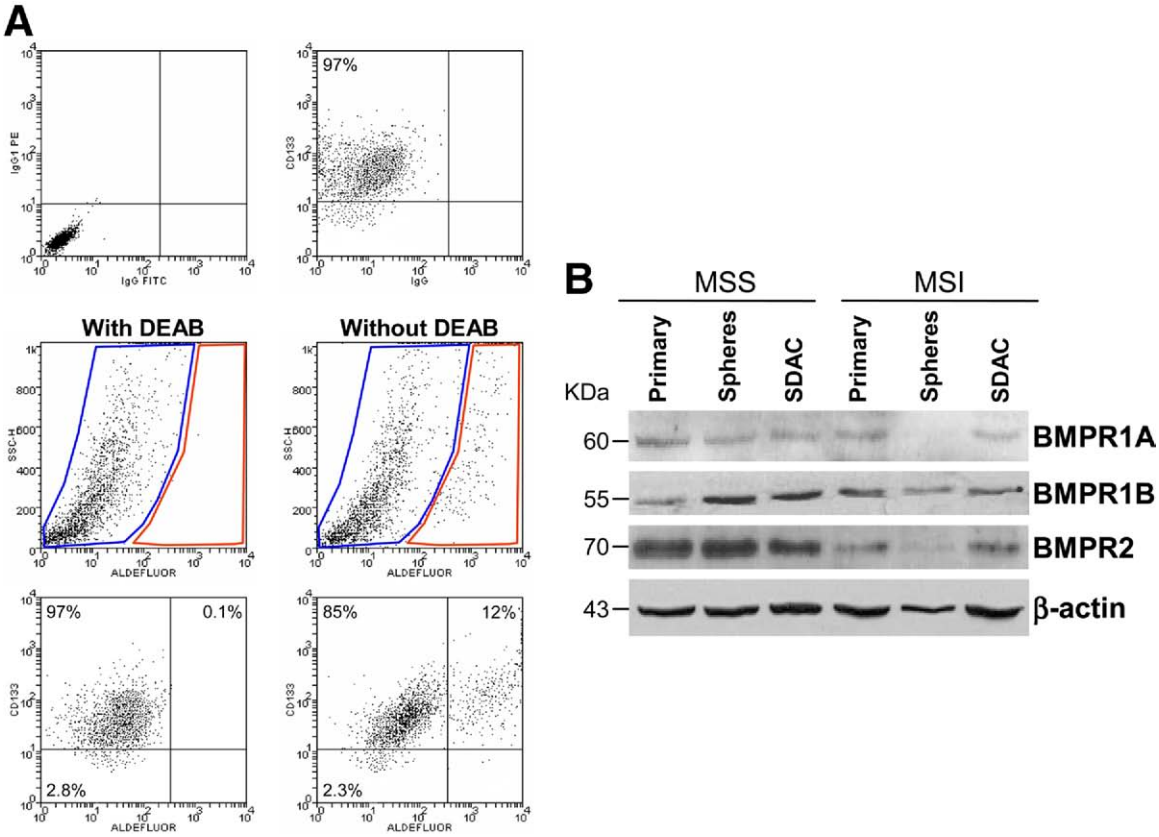

Supplementary Figure 1. (*A*) ALDEFLUOR assay on CRC spheres. Dissociated sphere cells exposed to ALDEFLUOR substrate (BODIPY-aminoacetaldehyde diethyl aceta) and the specific ALDH inhibitor diethylaminobenzaldehyde were used to define the CD133-positive population with high ALDH activity (*red region*) and the population with low ALDH activity (*blue region*). One representative of 20 CRC sphere cultures derived from different tumors is shown. (*B*) Representative immunoblot analysis of BMPR1A, BMPR1B, and BMPR2 on primary tumor cells (*Primary*), sphere cells (*Spheres*), and SDACs derived from MSS (patient number 14) and MSI (patient number 3) tumors. Loading control was assessed by β-actin.

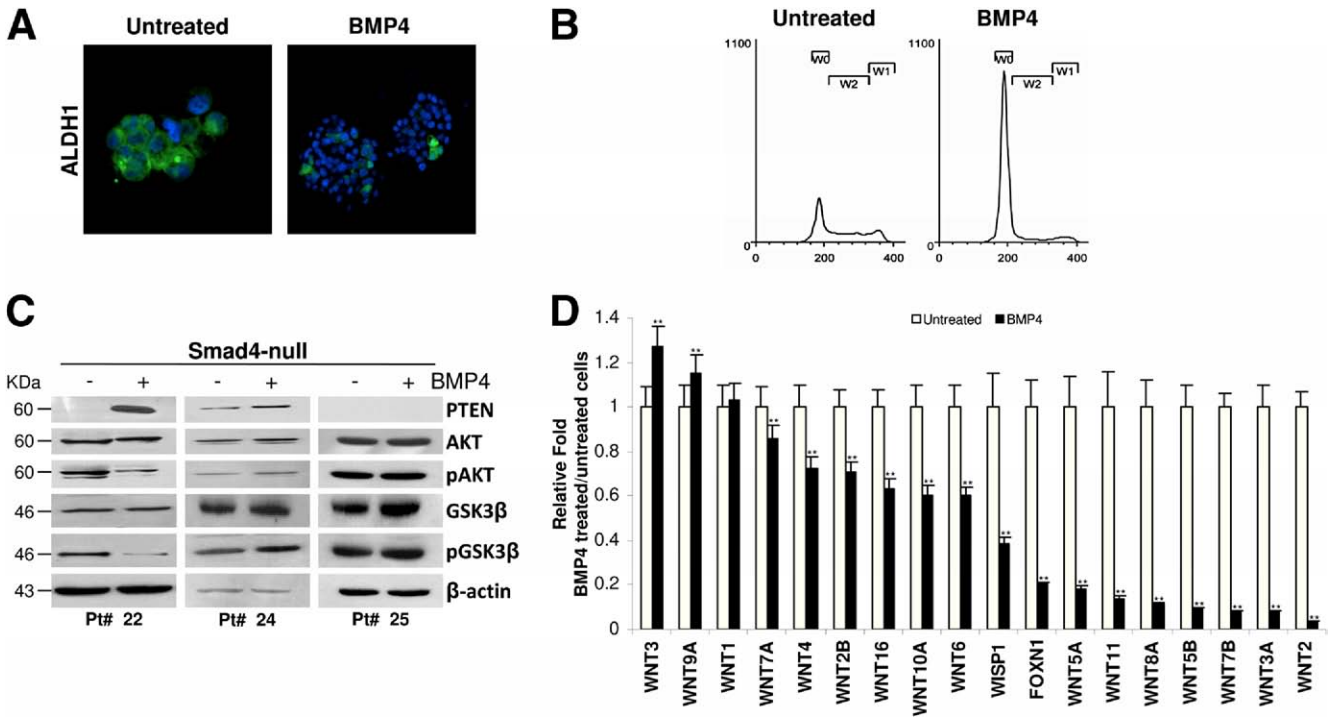

Supplementary Figure 2. (*A*) Confocal microscopy analysis of ALDH1 (*green color*) of sphere cells untreated or treated with BMP4 for 6 days. Nuclei were counterstained by Toto-3 (*blue color*). (*B*) Representative cell-cycle profile of dissociated sphere cells after 48 hours exposure to vehicle alone (*Untreated*) or BMP4. (*C*) Representative immunoblot analysis of PTEN, AKT, pAKT, GSK3β, and pGSK3β on sphere cells, derived from 3 different Smad4-null patients (patient numbers 22, 24, and 25), untreated and treated with BMP4. Loading control was assessed by β-actin. (*D*) Relative fold of expression levels of Wnt-related gene in sphere cells treated for 48 hours with BMP4 vs untreated sphere cells. Glyceraldehyde-3-phosphate dehydrogenase (*GAPDH*) was used as endogenous control. Data are expressed as mean ± standard deviation of 10 independent experiments (patient numbers 2–4, 11, 13–17, and 19).